The Wounded Forge

Anti-Closure, Calibrated Stress, and Metastability in Complex Adaptive Systems

tratium

Abstract. We proposed that systems under stress either fragment or reorganize at higher capacity, and that a two-parameter phase diagram — anti-closure (α) versus stress load (σ) — determines which outcome occurs. Three computational experiments tested the framework. The central prediction — a unimodal stress-tolerance curve $\sigma_{\text{crit}(\alpha)}$ — was falsified: the Kuramoto sweep showed σ_{crit} is monotonically decreasing, because high noise tolerance in rigid systems reflects inertia, not developmental bandwidth. The revised framework uses metastability ($\text{Var}(r)$) rather than coherence ($\langle r \rangle$) as the growth-zone measure and finds a bounded metastability island in the (α, σ) plane whose topology matches the predicted nine-cell structure. A coupling-strength sweep across nine K values shows this island persists as a three-dimensional surface ($r(K, \Delta\omega_{\text{centroid}}) = 0.94$, $r(K, \eta_{\text{centroid}}) = 0.98$). An Arnold circle-map test reproduces the Diophantine hierarchy for deterministic resonance: the golden ratio ($K_{\text{crit}} = 0.245$) resists locking 40% longer than the silver ratio (0.176), while rationals lock at the first nonzero coupling — but this advantage vanishes under stochastic noise in bulk populations, resolving the φ-specificity question as domain-dependent. We ground α in KAM theory and coordination dynamics; ground σ in hormesis, allostatic load, and antifragility theory; bridge them through a hormesis-antifragility correspondence (hormesis supplies the empirical curve; antifragility supplies the local curvature criterion via Jensen's inequality); and identify recovery time τ as a domain-specific calibration condition. The formal pattern recurs across cellular, organismic, and collective scales — the same mathematical structure, though not necessarily the same mechanism. Intelligence is not produced by stability. It is produced by metastability under disciplined perturbation.

Keywords: metastability, anti-resonance, hormesis, antifragility, phase transitions, golden ratio, Kuramoto model, KAM theory, coordination dynamics, Diophantine conditions, chimera states, collective intelligence

---

1 Introduction

1.1 The Two Problems

Two problems have been studied independently across complexity science, neuroscience, and biology. The first is the maintenance problem: how do living systems resist collapse into pathological order (seizure, rigidity, crystallization) or dissolution into chaos (fibrillation, fragmentation, noise)? The second is the development problem: how does stress produce growth in some systems and destruction in others? This paper argues these are not separate problems. They are two axes of a

single phase diagram whose interaction determines whether a complex adaptive system stagnates, develops, or fragments.

The maintenance problem has been addressed by criticality theory (Bak, Tang, & Wiesenfeld, 1987; Muñoz, 2018), anti-resonance in dynamical systems (Greene, 1979; Arnold, 1961), and coordination dynamics (Kelso, 2021). The development problem has been addressed by hormesis (Calabrese, 2004), antifragility (Taleb & Douady, 2013), post-traumatic growth theory (Seery, Holman, & Silver, 2010), and stress-sharing in collective intelligence (Shreesha & Levin, 2024). No published work has unified these two axes into a single framework with falsifiable predictions and computational evidence.

We introduce two coupled parameters: α (the anti-closure index, measuring structural resistance to premature synchronization) and σ (the stress load, measuring perturbation intensity). We show that development occurs only in a bounded zone of $\alpha \times \sigma$ space, characterized not by high coherence but by high metastability — the regime Kelso (2021) identifies as the operating mode of living systems, where the system tends toward both coordination and independence without being captured by either.

Three computational experiments test the framework. The results partially falsify the original prediction and support the revised formulation — a sequence we report in full.

1.2 Methodological Note

This paper does not treat traditional accounts of incompletion, wound, remainder, and sacred proportion as decorative metaphors appended to a scientific argument. It treats them as historically prior recognitions of a formal pattern: generativity through structured non-closure. The Pythagorean discovery that the circle of fifths does not close, the alchemical insistence that the Stone has a remainder, the Islamic geometric tradition of the deliberate flaw, the Japanese aesthetic of *wabi-sabi*, the Hermetic teaching that the Work is never finished — these are not ornamental precursors to the mathematics that follows. They are the reason this investigation exists. The mathematical sections specify one precise version of the pattern through Diophantine incommensurability and anti-resonance; the computational sections test where that mechanism is actually instantiated; the cross-domain observations ask how far the pattern extends. The claim is neither reductive materialism nor free symbolic association, but a testable formalization of an older intuition: that living systems are built to resist their own closure. Whether the older traditions tracked the same dynamical structure or a family resemblance is left open; the mathematical sections specify one precise version of the pattern and the computational sections test where it is actually instantiated.

2 Mathematical Foundations: Anti-Closure

2.1 KAM Theory and the Last Barrier

The Kolmogorov-Arnold-Moser (KAM) theorem addresses the fate of quasi-periodic orbits in Hamiltonian systems under perturbation. Consider an integrable Hamiltonian system whose phase

space is foliated by invariant tori on which motion is quasi-periodic with frequency vector $\boldsymbol{\omega} = (\omega_1, ..., \omega_n)$. The KAM theorem states that for sufficiently small perturbations, tori whose frequency ratios satisfy a Diophantine condition

$$|\boldsymbol{\omega} \cdot \boldsymbol{k}| \geq \frac{C}{|\boldsymbol{k}|^\tau} \quad \text{for all } \boldsymbol{k} \in \mathbb{Z}^n \setminus \{\mathbf{0}\}$$

persist as slightly deformed tori (Kolmogorov, 1954; Arnold, 1963; Moser, 1962). The Diophantine condition excludes frequency vectors "too close" to rational — those susceptible to resonance. Tori with rational frequency ratios are destroyed first; the more irrational the ratio, the more robust the torus.

The golden ratio $\varphi = \frac{1+\sqrt{5}}{2} \approx 1.618$ has the continued fraction representation $[1; 1, 1, 1, ...]$ — the smallest possible partial quotients at every position, producing the slowest convergence of any continued fraction (Hardy & Wright, 1938). It is the extremal member of the **noble numbers** — irrationals whose continued fractions end in an infinite tail of ones — all of which share enhanced resistance to rational approximation. φ is the most resistant, but the property is graded, not binary.

Greene (1979) showed that in the Chirikov standard map, the golden-mean torus is the last quasi-periodic invariant circle to be destroyed as perturbation increases — the last barrier between ordered and chaotic dynamics. MacKay (1983) and Fox & Meiss (2019) supported this numerically to high precision.

2.2 Arnold Tongues and Anti-Resonance

In driven oscillator theory, Arnold tongues (Arnold, 1961) are the wedge-shaped regions in parameter space where a forced oscillator locks onto the driving frequency at a rational ratio p/q. Between the tongues lie gaps where the oscillator maintains quasi-periodic motion. The golden ratio sits at the center of the widest gap — the frequency ratio most resistant to locking.

For biological systems composed of coupled oscillators — neurons, cardiac pacemakers, circadian clocks — this result has direct consequences. A system whose component oscillators are tuned to noble-ratio frequencies is maximally resistant to pathological synchronization while still permitting weak coupling for coordination. Pletzer et al. (2010) demonstrated that the canonical EEG frequency bands (δ, θ, α, β, γ) are separated by factors approximating φ, and that oscillators at φ-ratio frequencies resist synchronization of their excitatory phases. Kramer (2022) formalized this as the "golden rhythms" framework: φ-spaced rhythms optimally support both multiplexing (segregation) and integration of neural information. A 2026 multi-dataset validation ($N = 320$; Ursachi et al., *Frontiers in Human Neuroscience*) reported the association between golden ratio organization in EEG and theta-alpha frequency convergence near the critical 8 Hz boundary.

2.3 Sturmian Words and Quasicrystals

The Fibonacci word — the canonical Sturmian word, generated by φ-rotation on the unit circle — achieves minimal aperiodic order: maximal structure without periodicity (Morse & Hedlund, 1938, 1940). Penrose tilings extend this to two dimensions: long-range order, five-fold symmetry, coherence without closure. The Aubry transition in the Frenkel-Kontorova model provides the material

analogue: golden-ratio atomic chains are the most resistant to pinning by a periodic substrate (Bylinskii et al., 2016, *Nature Materials*). These are all instances of the same formal property: φ-structured incommensurability produces maximal order without periodicity — coherent but not locked.

3 Stress-Driven Development

3.1 Hormesis as Empirical Curve

Hormesis — the biphasic dose-response in which low-dose stress improves function while higher doses impair it — is now recognized as a general biological phenomenon. Calabrese and Blain (2005) documented hormetic responses across chemical classes, models, and endpoints. The hormetic zone is consistent: stimulatory responses typically peak at 130–160% of control at doses below the NOAEL. Molecular mechanisms include heat shock protein upregulation (Calabrese et al., 2015), mitochondrial biogenesis via reactive oxygen species (Ristow & Schmeisser, 2014), and autophagy activation under caloric restriction (Mattson, 2008; Masoro, 2007; Spadaro et al., 2022).

Exercise provides the clearest demonstration. Moderate exercise generates ROS that upregulate endogenous antioxidant defenses and mitochondrial biogenesis. Antioxidant supplementation **blocks** these adaptations — demonstrating that the stress itself, not just the activity, is the necessary signal (Ristow & Schmeisser, 2014). Trained immunity via BCG vaccination produces enhanced innate immune responses months to years after inoculation through epigenetic reprogramming of monocytes (Arts et al., 2018) — a long-duration hormetic effect at the immune system level.

3.2 Antifragility as Curvature Criterion

Taleb and Douady (2013) defined antifragility mathematically: a system is antifragile if its transfer function is locally convex in the domain of stressors. By Jensen's inequality, a system with a convex response function benefits from stress variability: $E[f(x)] > f(E[x])$ when f is convex.

Hormesis and antifragility address the same empirical territory at different levels of formalization. Hormesis supplies the empirical dose-response curve; antifragility supplies the curvature criterion for when stress variability improves expected function. Specifically, the hormetic dose-response curve has a region of positive curvature (concave-up, antifragile) at low doses and negative curvature (concave-down, fragile) at higher doses. The inflection point marks the transition. Below it, variable dosing at a fixed mean improves expected outcomes (Jensen favors convexity). Above it, variable dosing worsens expected outcomes (Jensen penalizes concavity). This correspondence, while structurally clear, has not been formally established in the peer-reviewed literature. The present paper proposes it as a bridge between the toxicological and mathematical treatments of the same underlying pattern.

A critical caveat: many hormetic curves are concave near their peak, meaning the antifragile regime is limited to the **ascending** portion, not the entire beneficial region. The framework predicts

local antifragility only where the fitted dose-response function is genuinely convex — a testable condition per domain.

3.3 Allostatic Load as Phase Transition

McEwen's allostatic load model (1998, 2017) provides the mechanism for the upper boundary of the stress-benefit curve. Allostasis — "stability through change" — becomes pathological when the stress response fails to deactivate: repeated stressors without recovery, failure to habituate, failure to terminate, or inadequate response triggering compensatory hyperactivation. The transition from adaptive allostasis to overload exhibits nonlinearity, attractor-like pathology, and hysteresis — recovery requires substantially more favorable conditions than the degradation that produced the damage (McEwen & Gianaros, 2011).

Heart rate variability serves as a candidate order parameter for this transition. HRV indexes autonomic flexibility — the system's capacity to modulate its state fluidly. High HRV places the system near the metastable regime; low HRV places it in the rigid (locked) phase. HRV decreases with allostatic load and predicts cardiovascular mortality, depression, and all-cause mortality (Thayer et al., 2010; Jarczok et al., 2015). The status of HRV as a strict thermodynamic order parameter is not yet established; the present paper treats it as a candidate whose status must be evaluated by the predictions in Section 7.

3.4 Stress Sharing and Bounded Coupling

Shreesha and Levin (2024) demonstrated computationally that stress sharing between cells — the leaking of stress molecules to neighbors — functions as cognitive glue for collective morphogenesis. The mechanism requires no altruism: each cell minimizes local stress, but the leaking signal bends the energy landscape for neighbors, inducing collective problem-solving. Stress sharing **enlarges the cognitive light cone** — the scale of goals the system can represent.

Stress coupling has a dark twin. Epileptic seizures are pathological hypersynchronization: Schmidt et al. (2014) showed the critical coupling threshold is significantly lower in epileptic brains. Cytokine storm, mass panic, and secondary traumatic stress (Sutton et al., 2022) are pathological coupling at immune, social, and organizational scales. The optimal regime requires bounded stress transmissibility: a coupling strength κ where too little produces isolation and too much produces collective seizure. The optimal κ is conditioned by anti-closure capacity — systems with stronger anti-resonant structure tolerate greater stress coupling before seizing.

4 The Two-Parameter Framework

4.1 Defining α and σ

The anti-closure index α measures structural resistance to premature synchronization, rigidification, or capture. Its formal correlates span domains: frequency disorder $\Delta\omega$ in the Kuramoto model, Diophantine exponent in KAM theory, frequency detuning in Kelso's HKB model, gap

width in Arnold tongue analysis, inverse epistatic connectivity $1/K$ in Kauffman's NK model, and disconnected-phase duration in Dual-Phase Evolution (Green, Paperin, & Sadedin, 2011).

The stress load σ measures perturbation intensity: external noise in the Kuramoto model, temperature in statistical mechanics, dose in hormesis, cumulative stress burden in allostatic load, disturbance magnitude in Holling's adaptive cycle, training load in exercise physiology.

4.2 The Nine-Cell Matrix

The interaction of α and σ produces a nine-cell phase diagram:

	Low σ	**Calibrated σ**	**Excessive σ**
Low α	Rigid stagnation	Brittle deformation	Collapse
Optimal α	Latent capacity	**Growth**	Fragmentation
Excessive α	Drift / incoherence	Unstable novelty	Chaos

Table 1: The $\alpha \times \sigma$ phase diagram. Growth occupies the center cell. Adjacent cells are operationally distinguishable: **rigid stagnation** (frozen order, zero variability); **brittle deformation** (global form preserved but accumulating cracks, slow recovery); **collapse** (catastrophic failure of rigid structure under stress); **latent capacity** (open but undeveloped); **fragmentation** (high variability, failed integration); **drift** (too decoupled for sustained structure); **unstable novelty** (constant change without consolidation); **chaos** (no coherent response). See the Kuramoto metastability heatmap (Experiment 1) for computational support of this topology.

The center cell is the only one that produces sustained development. Its boundedness is the framework's primary prediction. The matrix is the interpretive scaffolding; the metastability island from the Kuramoto sweep (Section 5) is the evidence. The eight surrounding cells are inferred from the island's boundary topology, not independently demonstrated in the present simulations.

4.3 Metastability, Not Criticality

Kelso's coordination dynamics (2021; Tognoli & Kelso, 2014) provides the correct vocabulary for the growth zone. Living systems do not operate at a critical point (requiring fine-tuning) or in a single attractor (precluding flexibility). They operate in a **metastable** regime — tending toward both phase-locking and independence without being captured by either. In the extended HKB model, frequency detuning $\delta\omega$ (our α) eliminates stable fixed points and produces the metastable regime: the system dwells near the ghosts of former attractors, visits multiple coordination states, and maintains simultaneous integration and segregation. Bansal et al. (2019) demonstrated chimera states — coexisting synchronized and desynchronized regions — in empirical human brain networks using functional MRI. This is arguably the cleanest empirical realization of the framework's central claim: the brain achieves simultaneous integration and segregation not by balancing at a critical point but by inhabiting a metastable regime where partial coordination coexists with structured independence. The chimera is anti-closure made visible.

Metastability, not criticality, is the claim. The system is not balanced at a knife's edge. It occupies a finite region of parameter space where anti-closure prevents capture and calibrated perturbation drives exploration.

4.4 Recovery

The growth zone exists only when a temporal condition is met: adequate recovery time τ between perturbation episodes. Let T_R denote available recovery time and $T_{C(\alpha,\sigma)}$ denote the system's characteristic consolidation time. Define $\tau = \frac{T_R}{T_{C(\alpha,\sigma)}}$. Growth requires $\tau \geq 1$: the next perturbation arrives after consolidation. McEwen's allostatic overload pathways are temporal failures: repeated hits without recovery, failure to habituate, failure to terminate. The supercompensation curve in exercise science (Viru, 1984) demonstrates that training benefit requires the next stressor during the recovery overshoot. Tononi and Cirelli's synaptic homeostasis hypothesis (2006) frames sleep as α-restoration: wakefulness injects σ (learning, perturbation), sleep selectively decouples and prunes (restoring anti-closure capacity).

4.5 Existing Frameworks as Projections

Several existing frameworks can be understood as single-parameter projections of the full $\alpha \times \sigma$ space. Langton's λ parameter (1990) controls rule disorder (an α slice without σ). Kauffman's NK model (1993) has structural parameters (N, K) without explicit stress. Holling's adaptive cycle (Gunderson & Holling, 2002) traces a qualitative trajectory **through** $\alpha \times \sigma$ space: r-phase in high-α/low-σ, K-phase in low-α/low-σ, Ω-phase in low-α/high-σ, α-phase in high-α/high-σ. Green, Paperin, and Sadedin's Dual-Phase Evolution (2011) is the closest relative — explicitly modeling connectivity oscillation — but uses a single parameter and does not formalize anti-resonance or hormetic curvature. No existing framework unifies Diophantine anti-locking with hormetic stress-response in a single model.

5 Computational Evidence

5.1 Experiment 1: The Kuramoto $(\Delta\omega, \eta)$ Sweep

We tested the framework in the canonical coupled oscillator model: $N = 200$ Kuramoto oscillators with coupling $K = 2.0$, swept across a 40×40 grid of frequency heterogeneity $\Delta\omega \in [0.1, 6.0]$ (the α axis) and external noise intensity $\eta \in [0.0, 4.0]$ (the σ axis), with three trials per grid point. Each trial integrated for $T = 500$ using Euler-Maruyama ($T_{\text{transient}} = 200$, $T_{\text{measure}} = 300$). We measured the time-averaged order parameter $\langle r \rangle$ (coherence) and its variance $\text{Var}(r)$ (metastability index).

Result 1a: The coherence-loss threshold σ_{crit} — the noise level at which $\langle r \rangle$ drops below 0.3 — is monotonically decreasing in α. This falsifies the original unimodal prediction. At low α, the system locks tightly and tolerates substantial noise. At high α, the system is never coherent. High noise tolerance for a rigid system is not developmental bandwidth; it is inertia.

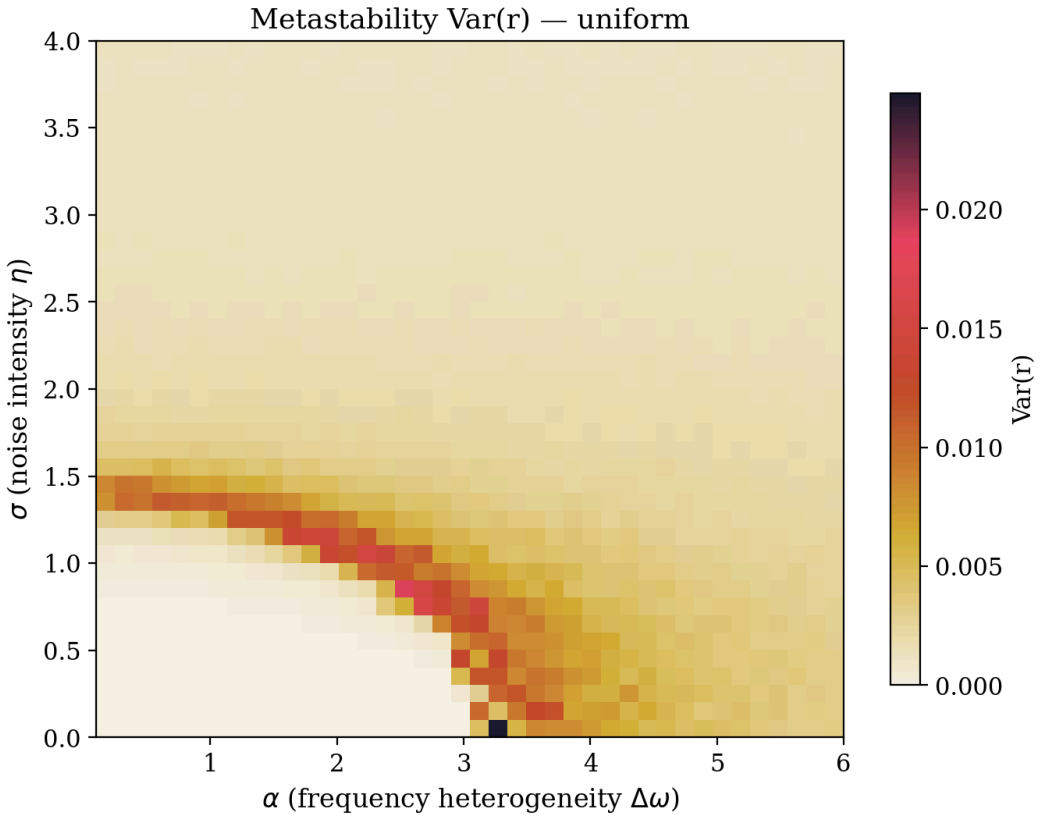

Figure 1: Metastability heatmap ($\mathrm{Var}(r)$) from the Kuramoto $(\Delta\omega, \eta)$ sweep at $K = 2.0$. The bounded diagonal island of high dynamical flexibility — where the system dwells near phase transitions without capture — occupies intermediate values of both α (frequency heterogeneity) and σ (noise intensity). This is the computational signature of the growth zone.

Result 1b: The metastability index $\mathrm{Var}(r)$ reveals a bounded diagonal island of high dynamical flexibility — the region where the system dwells near phase transitions, visiting multiple coordination states without capture. This island occupies intermediate values of both α and σ, consistent with the growth cell of the nine-cell matrix. Below the island: rigidity or stable incoherence (low variance). Above: noise-dominated disorder (low variance). The island is bounded on all sides.

5.2 Experiment 2: The Coupling-Strength Sweep

To test whether the metastability island is a single-K artifact, we swept coupling strength across nine values ($K \in [0.5, 4.5]$) on a coarser 20×20 $(\Delta\omega, \eta)$ grid with three trials per point. For each K, we identified the island's centroid (top-5% $\mathrm{Var}(r)$ cells).

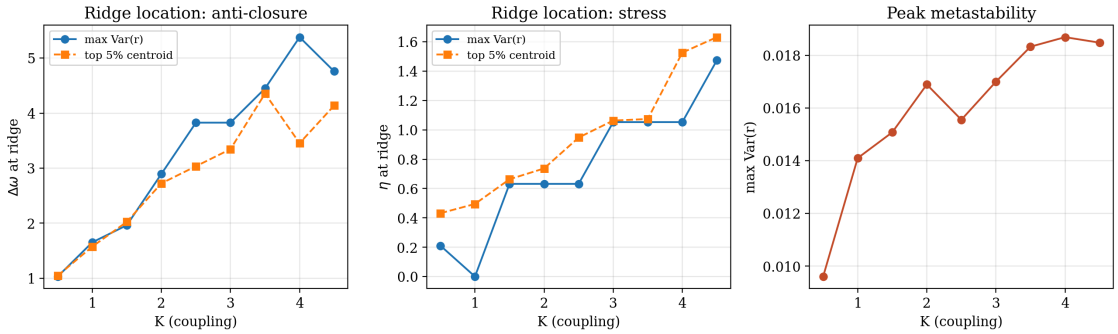

Figure 2: Metastability ridge across coupling strength. Left: $\Delta\omega$ at ridge vs. K. Center: η at ridge vs. K. Right: peak $\mathrm{Var}(r)$ vs. K. The ridge shifts linearly with coupling ($r = 0.94$, 0.98), demonstrating a three-dimensional metastability surface.

The metastability ridge persists across all coupling strengths and shifts predictably: as K increases, the ridge moves toward higher $\Delta\omega$ and higher η. Stronger coupling requires more anti-closure to prevent locking and tolerates more noise before fragmentation. The correlations between K and ridge centroid coordinates are $r(K, \Delta\omega_{\text{centroid}}) = 0.94$ and $r(K, \eta_{\text{centroid}}) = 0.98$. The metastability island is not a two-dimensional ridge but a surface in the three-dimensional $(K, \Delta\omega, \eta)$ space — a structural feature of the parameter space, not an artifact of a single slice.

5.3 Experiment 3: The Arnold Circle-Map Test

The Kuramoto sweep showed that frequency distribution type (uniform, φ-spaced, harmonic) produces nearly identical results under stochastic noise. This null prompted a targeted test of the actual anti-resonance claim: resistance to **deterministic** resonance locking. We used the standard circle map — the canonical Arnold tongue system — sweeping coupling $K \in [0, 1.2]$ at 500 points for seven frequency ratios: φ (golden), the silver ratio, $\sqrt{2}/2$, $1/\pi$, and three rationals (3/5, 2/3, 5/8).

The Diophantine hierarchy is reproduced:

Ratio	K_{crit}	**% unlocked**	**Class**
φ (golden)	0.245	76.0%	Noble (extremal)
σ_s (silver)	0.176	71.4%	Noble
$\sqrt{2}/2$	0.063	69.0%	Irrational, non-noble
$1/\pi$	0.034	67.6%	Transcendental
3/5	0.000	70.8%	Rational
2/3	0.000	71.4%	Rational
5/8	0.000	68.4%	Rational

Table 2: Arnold tongue test. K_{crit}: coupling at first locking. φ requires 40% more coupling than silver before first locking; rationals lock at the first nonzero coupling under this detection criterion.

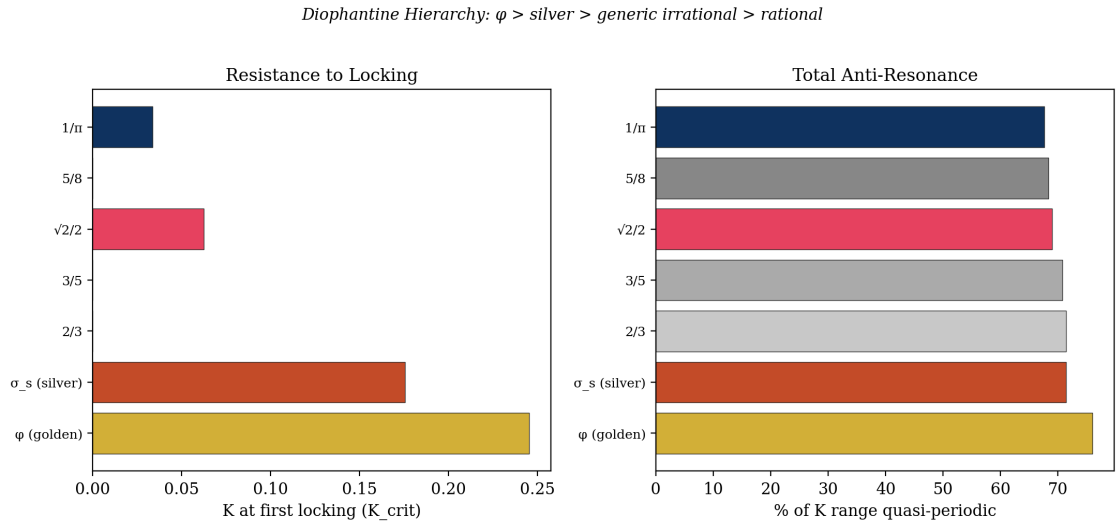

Figure 3: Arnold tongue test: resistance to deterministic resonance locking by frequency ratio. Left: K_{crit} (coupling at first locking). Right: fraction of K range remaining quasi-periodic. The noble number hierarchy ($\varphi >$ silver $>$ generic irrational $>$ rational) holds for K_{crit}.

The golden ratio resists deterministic locking onset longer than any other ratio tested. The noble hierarchy holds: $\varphi >$ silver $>$ generic irrational $>$ rational. Rationals lock at the first nonzero coupling.

5.4 Resolution: Domain-Specific Anti-Resonance

The two simulation types resolve the φ-specificity question precisely. Noble-ratio anti-resonance is real for **deterministic resonance capture** (Arnold tongues, KAM torus destruction) and null for **stochastic noise tolerance** in bulk populations. φ protects against lock-in, not against random perturbation. The anti-closure parameter α in the present framework corresponds to resistance to deterministic capture — the regime where the Diophantine hierarchy operates.

5.5 What the Simulations Did to the Framework

The original prediction — unimodal $\sigma_{\text{crit}(\alpha)}$, growth as a coherence peak — was wrong. The simulation falsified the specific form and motivated a revision. The revised framework uses metastability ($\text{Var}(r)$) rather than coherence ($\langle r \rangle$) as the growth-zone measure. This is a different and weaker claim than the original, but it is supported by the data. The metastability island, the coupling-dependent ridge, and the Diophantine hierarchy are empirical findings; the nine-cell matrix and the $\alpha \times \sigma$ framework are the interpretive structure they support. The predictive power of the framework is lower than it appeared in v1 — the specific form of $\sigma_{\text{crit}(\alpha)}$ was wrong — but the general topology (bounded growth zone, failure modes on all sides) survived.

6 Cross-Domain Observations

The mathematical core of this paper concerns anti-resonance and stress-response in coupled oscillatory systems. The following observations extend the pattern to biological and physical systems,

organized by evidential strength. The formal pattern recurs across these domains; whether a single mechanism underlies all instances is an open question the cross-scale predictions in Section 7 are designed to test.

6.1 Tier 1: Direct Mathematical Instantiation

KAM/Arnold tongue dynamics (Sections 2–3 and the computational results) provide the strongest evidence: anti-resonance, resonance locking, and the Diophantine hierarchy are established mathematical results reproduced computationally in the present circle-map test. **Engineered anti-closure** — golden-angle MRI sampling (Winkelmann et al., 2007), Aubry transition in atomic chains (Bylinskii et al., 2016) — demonstrates that the anti-resonance property is exploitable in designed systems.

6.2 Tier 2: Biological Systems with Measured Signatures

Brain criticality. Neuronal avalanches follow power-law distributions consistent with near-critical dynamics (Beggs & Plenz, 2003). Consciousness is associated with near-critical cortical electrodynamics (Toker et al., 2022, *PNAS*). Daniels et al. (2018, *Physical Review Letters*) showed biological regulatory networks are closer to criticality than random networks. However, Touboul and Destexhe (2017) demonstrated that power-law statistics and universal scaling can arise in the absence of criticality — power laws are insufficient evidence for a critical point, not merely imprecise fits, and Sipling, Zhang, and Di Ventra (2026, arXiv:2604.21071) argue the critical point may not exist — broader memory-induced long-range-order phases could explain the data. The brain criticality hypothesis is active, not settled.

Neural frequency architecture. EEG frequency bands approximate φ-spacing (Pletzer et al., 2010; validated by Ursachi et al., 2026, $N = 320$). The association is robust but correlational. The causal claim — that φ-spacing **maintains** criticality — requires the experimental manipulation proposed in Section 7 and has not been performed.

Phyllotaxis. The φ-angle packing of leaves and seeds arises from auxin-transport self-organization where each new primordium forms at the point of lowest inhibition (Reinhardt et al., 2003; Godin et al., 2022). This is a φ-instantiation, but the mechanism (inhibition geometry) differs from Arnold tongue anti-resonance to a forcing frequency — a different mathematical route to the same constant.

Collective animal behavior. Starling flocks exhibit scale-free behavioral correlations: correlation length scales with flock size (Cavagna et al., 2010, *PNAS*), the hallmark of a system near a phase transition. At the evolutionary scale, Ibbotson, Jimenez-Romero, and Page (2022, *Behavioral Ecology*) showed through agent-based modeling that only cooperative foraging phenotypes survive the harshest environments, but cooperative groups pay a penalty for miscoordination in benign conditions — the population-scale U-curve. Torney, Berdahl, and Couzin (2011) demonstrated that collective sensing in animal groups is optimized at intermediate coupling: too little and individuals cannot pool information; too much and the group locks into premature consensus. This is the bounded-coupling (κ) prediction instantiated in empirical collective behavior.

Stress sharing. Levin and Shreesha (2024) demonstrated computationally that stress sharing enlarges collective cognitive light cones and improves morphogenetic accuracy. Cancer, in Levin's framework, is a failure of collective intelligence: cells disconnected from the bioelectric information field revert to unicellular behavior (Chernet & Levin, 2013, 2014; Levin, 2024, *Communications Biology*).

Allostatic load and HRV. The transition from adaptive allostasis to overload is characterized by nonlinear dynamics and hysteresis (McEwen, 1998, 2017). HRV indexes autonomic flexibility and predicts health outcomes across domains (Thayer et al., 2010; Jarczok et al., 2015).

Seery's adversity U-curve. In a nationally representative sample ($N = 2,398$), people with moderate lifetime adversity showed better mental health outcomes than those with either no adversity or high adversity (Seery et al., 2010). This is the organismic hormesis curve. Self-reported post-traumatic growth is less reliable: Boals (2023) argues genuine PTG is rare and most self-reports reflect positive cognitive biases rather than actual development.

Protein marginal stability. Globular proteins maintain folding free energy of only 5–15 kcal/mol — too stable and they cannot undergo conformational changes; too unstable and they unfold. Marginal stability is the molecular edge of chaos (Taverna & Goldstein, 2002).

6.3 Tier 3: Structural Analogues

Genomic error rate. DNA polymerase error rate ($\sim 10^{-8}$ to 10^{-10}) is tuned, not minimized: too low $\rightarrow$ no evolution; too high $\rightarrow$ error catastrophe (Eigen, 1971). The error threshold is a formal phase transition. **Ecosystem disturbance.** The intermediate disturbance hypothesis (Connell, 1978) is intuitive but empirically contested (Fox, 2013). **Cosmological asymmetry.** Baryon asymmetry — one excess particle per billion — is the reason matter exists. It operates through CP violation, not anti-resonance; it is included as a structural parallel, not a mechanism claim. **Cardiac φ-ratios.** Yalta et al. (2016) reported φ-ratio spacing in cardiac intervals, but the evidence is correlational and the publication venue does not carry the same weight as the neural literature.

7 Predictions

The framework generates testable predictions:

1. **Metastability island**: In coupled oscillator networks, the regime of maximal dynamical flexibility should occupy a bounded island in the (α, σ) plane, identifiable by high $\mathrm{Var}(r)$ or equivalent metastability measures. The Kuramoto simulation supports this; the prediction extends to neural, cardiac, and synthetic networks.
2. **α-dependent metastability bandwidth**: Systems with intermediate anti-closure should access the widest range of σ values compatible with metastable dynamics. The coupling-strength sweep shows this bandwidth shifts with K.
3. **Deterministic vs. stochastic regime separation**: Noble-ratio frequency spacing should improve anti-locking under deterministic coupling (Arnold tongues) but not under additive

stochastic noise. The simulation supports this distinction and it should replicate in biological oscillator preparations.

4. **Bounded coupling**: Enhancing stress propagation beyond a threshold should produce collective overload. The threshold should be higher for systems with greater anti-closure capacity.
5. **Recovery necessity**: Intermittent stress with recovery should outperform continuous stress at the same mean intensity — testable in exercise (interval vs. continuous), fasting (intermittent vs. chronic restriction), and neural stimulation (pulsed vs. continuous).
6. **Cross-scale consistency**: Interventions increasing α at one scale (e.g., vagal stimulation $\rightarrow$ cardiac HRV) should increase σ-tolerance at adjacent scales. If this fails, the scale-invariance claim is falsified.
7. **Chimera states as growth-zone signature**: The spatial signature of the growth zone in extended systems should be chimera-like: coexisting coherent and incoherent domains.

8 Discussion

8.1 Limitations

The framework's primary risk is overextension. The α and σ parameters are defined by structural analogy across domains, not by a single measured quantity. The claim that Kuramoto frequency disorder, Diophantine exponents, HKB detuning, and NK connectivity index the **same underlying dimension** is an assumption the cross-scale predictions are designed to test. If increasing α in one domain does not widen σ-tolerance in adjacent domains, the scale-invariance claim is falsified. The formal pattern recurs; the mechanism may not.

The simulations use all-to-all Kuramoto coupling ($N = 200$, 3 trials per cell) and the standard circle map. These are canonical models, not biological systems. The sample size ($N = 200$, three trials per cell) is thin for variance estimates — $\mathrm{Var}(r)$ is itself a variance, and three trials provide limited precision on its value. The $r = 0.94/0.98$ correlations in Experiment 2 would likely show wider confidence bands with bootstrap resampling. The metastability island in a Kuramoto model does not prove the existence of a metastability island in cortical networks or immune systems. The computational results establish that the mathematical structure works in the canonical model — a necessary but not sufficient condition for the biological claims.

$\mathrm{Var}(r)$ is a standard but incomplete metastability index. Dwell-time distributions, Lempel-Ziv complexity, and metastability indices in the Deco-Kelso sense would provide more robust characterization of the growth zone. A deeper concern, tested directly: any model with a phase transition will produce a $\mathrm{Var}(r)$ peak at the boundary. We ran the control experiment — a Kuramoto system with **identical** frequencies ($\Delta\omega = 0$, zero anti-closure) and noise swept across $\eta \in [0, 4]$ with 10 trials per point. The result: the $\mathrm{Var}(r)$ peak **exists** at $\Delta\omega = 0$ ($\mathrm{Var}(r)_{\mathrm{peak}} = 0.011$ at $\eta \approx 1.37$). The metastability island is therefore a generic phase-transition crossover signature, not specific evidence for the anti-closure framework.

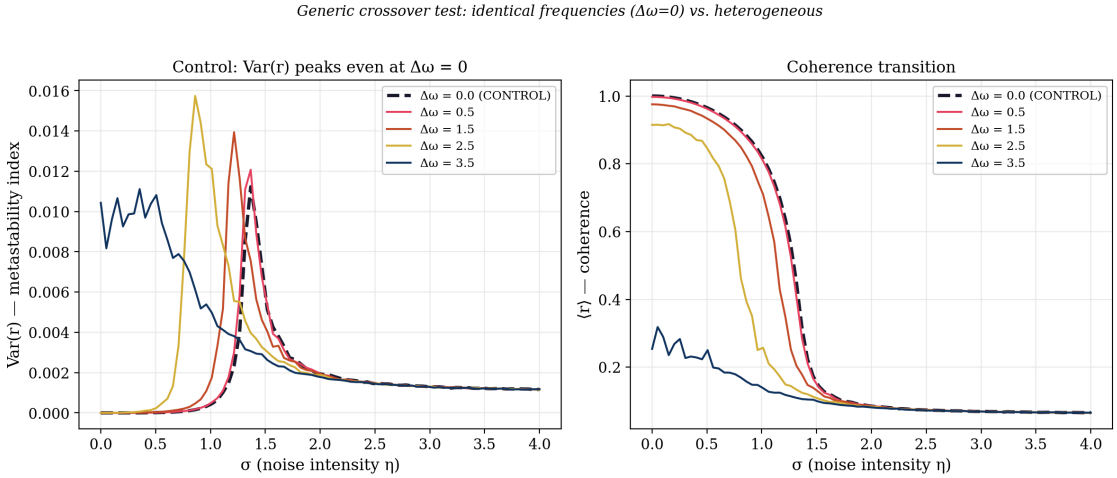

Figure 4: Control experiment. Left: Var(r) versus noise for identical frequencies ($\Delta\omega = 0$, dashed) and four heterogeneous cases. The Var(r) peak exists even without anti-closure. Right: corresponding coherence curves. Anti-closure shifts the peak location and increases its height (40% taller at $\Delta\omega = 2.5$) but does not create it.

However, anti-closure **modulates** the peak: intermediate $\Delta\omega$ increases peak height by 40% (0.016 at $\Delta\omega = 2.5$ vs. 0.011 at $\Delta\omega = 0$), shifts its location along the η axis, and sharpens its profile. The revised claim is therefore narrower than the original: anti-closure does not **produce** the metastability regime — it **tunes** its position, intensity, and shape within a generic phase-transition landscape. A system with anti-closure accesses a more pronounced and differently located metastability zone than an identical system without it. Whether this quantitative modulation is sufficient to justify the framework's qualitative claims about developmental bandwidth is an open question the present simulations raise but do not resolve.

The recovery parameter $\tau = \frac{T_R}{T_{C(\alpha,\sigma)}}$ is operationalized as a ratio but T_C has no domain-general empirical estimates. Return-to-baseline HRV, autocorrelation decay, supercompensation timing, and inflammatory marker normalization are candidate measures per domain; none has been validated as a universal consolidation-time metric.

The hormesis literature inherits standard criticisms: uncertain generalizability, post-hoc curve selection, incomplete mechanistic grounding, and unsuitability as a default in human risk assessment (Thayer et al., 2005; Mushak, 2007). The narrower claim — that some biological stress responses are locally convex — is well-supported; the broader claim that hormesis is universal is not.

The civilizational extension — Mühlmann's MSC, Holling's adaptive cycle, Turchin's secular cycles as trajectories through $\alpha \times \sigma$ space — is a structural hypothesis, not an established result.

The original unimodal $\sigma_{\text{crit}(\alpha)}$ prediction was falsified by the Kuramoto sweep. The revised framework (metastability island via Var(r)) is a different and weaker claim. The framework's predictive power is lower than it appeared in v1.

8.2 Relation to Existing Frameworks

Taleb's antifragility (2012) provides the conceptual vocabulary but lacks biological formalization; the present paper supplies the hormesis bridge and the curvature criterion. Prigogine's dissipative structures (1977) establish the thermodynamic precondition (far-from-equilibrium); the present framework adds the informational complement (anti-closure maintains the near-critical regime). Levin's TAME framework (2022) provides the biological foundation for multiscale intelligence; the present paper extends it by proposing stress as a mechanism for cognitive light cone enlargement. Friston's free energy principle (2010) also addresses self-organization and active inference, but the frameworks disagree about something substantive. FEP holds that living systems minimize surprise — that the organism acts to reduce the divergence between its predictions and its sensory input. The present framework holds that living systems **import** surprise within bounds — that calibrated perturbation is developmentally necessary, and that a system that successfully minimizes all surprise has entered the rigid-stagnation cell, not the growth cell. These are different claims about what living systems **do**, not different formalisms for the same process. Green et al.'s Dual-Phase Evolution (2011) is the closest structural relative, differing primarily in its single-parameter structure and absence of the anti-resonance formalism. Kauffman (1993), Langton (1990), and Holland (1992) provide the complex adaptive systems foundations on which the present framework builds.

8.3 The Design Principle

If the framework is correct, it suggests: **living systems are built to resist their own closure.** The golden ratio is not an ornament of nature but the canonical extreme of a broader class of anti-closure structures — noble-ratio anti-resonance, Diophantine incommensurability, structured incompletion — that prevent complex systems from collapsing into the ordered attractors that would end their development. The heartbeat varies because rigid regularity would be maladaptive. The genome errs because perfect fidelity would preclude evolution. The brain avoids global synchrony because lock-in would extinguish the flexibility on which cognition depends. Stress is not merely damage to be minimized. Under constrained conditions — sufficient anti-closure, calibrated dose, adequate recovery — stress is the developmental fire that expands coherence across scales. Anti-closure maintains the possibility-space. Stress provides the perturbation. Recovery consolidates the result. Intelligence is not produced by stability. It is produced by metastability under disciplined perturbation.

References

Arnold, V.I. (1961). "Small denominators. I: Mappings of the circumference onto itself." *Izv. Akad. Nauk SSSR Ser. Mat.* 25: 21–86.

Arnold, V.I. (1963). "Proof of A.N. Kolmogorov's theorem on the preservation of quasi-periodic motions under small perturbations of the Hamiltonian." *Russian Mathematical Surveys* 18.5: 9–36.

Arts, R.J.W. et al. (2018). "BCG vaccination protects against experimental viral infection in humans through the induction of cytokines associated with trained immunity." *Cell Host & Microbe* 23.1: 89–100.

Avramiea, A.-E. et al. (2022). "Long-range amplitude coupling is optimized for brain networks that function at criticality." *Journal of Neuroscience* 42.11: 2221–2233.

Bak, P., Tang, C., Wiesenfeld, K. (1987). "Self-organized criticality: An explanation of the 1/f noise." *Physical Review Letters* 59.4: 381–384.

Bansal, K. et al. (2019). "Cognitive chimera states in human brain networks." *Science Advances* 5.4: eaau8535.

Beggs, J.M. & Plenz, D. (2003). "Neuronal avalanches in neocortical circuits." *Journal of Neuroscience* 23.35: 11167–11177.

Boals, A. (2023). "Illusory posttraumatic growth is common, but genuine posttraumatic growth is rare." *Clinical Psychology Review* 103: 102301.

Bylinskii, A. et al. (2016). "Observation of Aubry-type transition in finite atom chains via friction." *Nature Materials* 15: 717–721.

Calabrese, E.J. (2004). "Hormesis: A revolution in toxicology, risk assessment and medicine." *EMBO Reports* 5(Suppl 1): S37–S40.

Calabrese, E.J. & Blain, R. (2005). "The occurrence of hormetic dose responses in the toxicological literature." *Toxicology and Applied Pharmacology* 202.3: 289–301.

Calabrese, V. et al. (2015). "Heat shock proteins and hormesis in the diagnosis and treatment of neurodegenerative diseases." *Immunity & Ageing* 12: 20.

Cavagna, A. et al. (2010). "Scale-free correlations in starling flocks." *PNAS* 107.26: 11865–11870.

Chernet, B.T. & Levin, M. (2013). "Transmembrane voltage potential is an essential cellular parameter for the detection and control of tumor development in a *Xenopus* model." *Disease Models & Mechanisms* 6.3: 595–607.

Connell, J.H. (1978). "Diversity in Tropical Rain Forests and Coral Reefs." *Science* 199.4335: 1302–1310.

Daniels, B.C. et al. (2018). "Criticality distinguishes the ensemble of biological regulatory networks." *Physical Review Letters* 121: 138102.

Deco, G., Kringelbach, M.L., Jirsa, V.K., & Ritter, P. (2017). "The dynamics of resting fluctuations in the brain: Metastability and its dynamical cortical core." *Scientific Reports* 7: 3095.

Eigen, M. (1971). "Selforganization of matter and the evolution of biological macromolecules." *Naturwissenschaften* 58.10: 465–523.

Fox, J.W. (2013). "The intermediate disturbance hypothesis should be abandoned." *Trends in Ecology & Evolution* 28.2: 86–92.

Fox, A. & Meiss, J.D. (2019). "Birkhoff averages and rotational invariant circles for area-preserving maps." *Physica D* 399: 1–14.

Friston, K. (2010). "The free-energy principle: A unified brain theory?" *Nature Reviews Neuroscience* 11: 127–138.

Godin, C. et al. (2022). "Modeling phyllotaxis: From the inhibition potential to the real plant." *Journal of Theoretical Biology* 547: 111183.

Green, D.G., Paperin, G., & Sadedin, S. (2011). "Dual phase evolution." *Journal of the Royal Society Interface* 8.58: 609–626.

Greene, J.M. (1979). "A method for determining a stochastic transition." *Journal of Mathematical Physics* 20.6: 1183–1201.

Gunderson, L.H. & Holling, C.S. (2002). *Panarchy: Understanding Transformations in Human and Natural Systems.* Island Press.

Hardy, G.H. & Wright, E.M. (1938). *An Introduction to the Theory of Numbers.* Oxford University Press.

Hatfield, E., Cacioppo, J.T., & Rapson, R.L. (1993). "Emotional contagion." *Current Directions in Psychological Science* 2.3: 96–100.

Holland, J.H. (1992). *Adaptation in Natural and Artificial Systems.* MIT Press.

Jarczok, M.N. et al. (2015). "Allostatic load and heart rate variability as health risk indicators." *Stress* 18.5: 550–558.

Kauffman, S.A. (1993). *The Origins of Order.* Oxford University Press.

Kelso, J.A.S. (2021). "Unifying large- and small-scale theories of coordination." *Entropy* 23.5: 537.

Kolmogorov, A.N. (1954). "On conservation of conditionally periodic motions under small perturbation of the Hamiltonian." *Doklady Akademii Nauk SSSR* 98: 527–530.

Kramer, M.A. (2022). "Golden rhythms as a theoretical framework for cross-frequency organization." *Neurons, Behavior, Data Analysis, and Theory.*

Langton, C.G. (1990). "Computation at the edge of chaos." *Physica D* 42.1-3: 12–37.

Levin, M. (2022). "Technological approach to mind everywhere." *Frontiers in Systems Neuroscience* 16: 768201.

Levin, M. (2024). "Collective intelligence: A unifying concept for integrating biology across scales and substrates." *Communications Biology* 7: 378.

MacKay, R.S. (1983). "A renormalization approach to invariant circles in area-preserving maps." *Physica D* 7: 283–300.

Masoro, E.J. (2007). "Role of hormesis in life extension by caloric restriction." *Dose-Response* 5.2: 163–173.

Mattson, M.P. (2008). "Dietary factors, hormesis and health." *Ageing Research Reviews* 7.1: 43–48.

McEwen, B.S. (1998). "Stress, adaptation, and disease: Allostasis and allostatic load." *Annals of the New York Academy of Sciences* 840: 33–44.

McEwen, B.S. (2017). "Allostasis and the epigenetics of brain and body health over the life course." *JAMA Psychiatry* 74.6: 551–552.

McEwen, B.S. & Gianaros, P.J. (2011). "Stress- and allostasis-induced brain plasticity." *Annual Review of Medicine* 62: 431–445.

Mora, T. & Bialek, W. (2011). "Are biological systems poised at criticality?" *Journal of Statistical Physics* 144: 268–302.

Morse, M. & Hedlund, G.A. (1938). "Symbolic dynamics." *American Journal of Mathematics* 60.4: 815–866.

Muñoz, M.A. (2018). "Colloquium: Criticality and dynamical scaling in living systems." *Reviews of Modern Physics* 90: 031001.

Pletzer, B. et al. (2010). "When frequencies never synchronize: the golden mean and the resting EEG." *Brain Research* 1335: 91–102.

Prigogine, I. (1977). Nobel Lecture: "Time, Structure and Fluctuations."

Reinhardt, D. et al. (2003). "Regulation of phyllotaxis by polar auxin transport." *Nature* 426: 255–260.

Ristow, M. & Schmeisser, K. (2014). "Mitohormesis." *Dose-Response* 12.2: 288–341.

Schmidt, H. et al. (2014). "Dynamics on networks: The role of local dynamics and global networks on the emergence of hypersynchronous neural activity." *PLoS Computational Biology* 10.11: e1003947.

Scheffer, M. et al. (2009). "Early-warning signals for critical transitions." *Nature* 461: 53–59.

Seery, M.D., Holman, E.A., & Silver, R.C. (2010). "Whatever does not kill us." *Journal of Personality and Social Psychology* 99.6: 1025–1041.

Shreesha, L. & Levin, M. (2024). "Stress sharing as cognitive glue for collective intelligences." *Biochemical and Biophysical Research Communications* 731: 150396.

Sipling, C., Zhang, Y.-H., & Di Ventra, M. (2026). "A critical assessment of the brain criticality hypothesis." arXiv:2604.21071.

Spadaro, O. et al. (2022). "Caloric restriction in humans reveals immunometabolic regulators of health span." *Science* 375.6581: 671–677.

Strogatz, S.H. (2000). "From Kuramoto to Crawford and back again." *Physica D* 143: 1–20.

Sutton, L. et al. (2022). "The contribution of organisational factors to vicarious trauma in mental health professionals." *European Journal of Psychotraumatology* 13.1: 2022278.

Taleb, N.N. & Douady, R. (2013). "Mathematical definition, mapping, and detection of (anti)fragility." *Quantitative Finance* 13.11: 1677–1689.

Tass, P.A. & Hauptmann, C. (2014). "Control of abnormal synchronization in neurological disorders." *Frontiers in Neurology* 5: 268.

Taverna, D.M. & Goldstein, R.A. (2002). "Why are proteins marginally stable?" *Proteins* 46.1: 105–109.

Thayer, J.F. et al. (2010). "Claude Bernard and the heart-brain connection." *Neuroscience & Biobehavioral Reviews* 33.2: 81–88.

Tognoli, E. & Kelso, J.A.S. (2014). "The metastable brain." *Neuron* 81.1: 35–48.

Torney, C., Berdahl, A., & Couzin, I.D. (2011). "Collective sensing and optimal group size." In *European Conference on Artificial Life*. MIT Press.

Toker, D. et al. (2022). "Consciousness is supported by near-critical slow cortical electrodynamics." *PNAS* 119.7: e2024455119.

Tononi, G. & Cirelli, C. (2006). "Sleep function and synaptic homeostasis." *Sleep Medicine Reviews* 10: 49–62.

Touboul, J. & Destexhe, A. (2017). "Power-law statistics and universal scaling in the absence of criticality." *Physical Review E* 95: 012413.

Ursachi, A. et al. (2026). "Golden ratio organization in human EEG is associated with theta-alpha frequency convergence: a multi-dataset validation study." *Frontiers in Human Neuroscience*. DOI: 10.3389/fnhum.2026.1781338.

Viru, A.A. (1984). "The mechanism of training effects: A hypothesis." *International Journal of Sports Medicine* 5: 219–227.

Winkelmann, S. et al. (2007). "An optimal radial profile order based on the Golden Ratio for time-resolved MRI." *IEEE Trans. Medical Imaging* 26.1: 68–76.

Yalta, K., Ozturk, S., Yetkin, E. (2016). "Golden Ratio and the heart: A review of divine aesthetics." *International Journal of Cardiology* 214: 107–112.